Neuronal Degeneration and Glial Activation in the Absence of Vascular Changes in Human Retinas of Patients With Diabetes

Henar Albertos-Arranz,[1] Natalia Martínez-Gil,[1] Xavier Sánchez-Sáez,[1] Julio Cesar Molina-Martín,[2] Pedro Lax,[1,3] and Nicolas Cuenca[1,3]

[1]Department of Physiology, Genetics and Microbiology, University of Alicante, Alicante, Spain
[2]Department of Ophthalmology, San Juan University Hospital, Alicante, Spain
[3]Alicante Institute for Health and Biomedical Research (ISABIAL), Alicante, Spain

Correspondence: Nicolas Cuenca, Department of Physiology, Genetics and Microbiology, University of Alicante, San Vicente del Raspeig Rd. W/N, Alicante 03690, Spain; cuenca@ua.es.

Received: October 3, 2024
Accepted: March 2, 2025
Published: March 25, 2025

Citation: Albertos-Arranz H, Martínez-Gil N, Sánchez-Sáez X, Molina-Martín JC, Lax P, Cuenca N. Neuronal degeneration and glial activation in the absence of vascular changes in human retinas of patients with diabetes. *Invest Ophthalmol Vis Sci.* 2025;66(3):53. https://doi.org/10.1167/iovs.66.3.53

Purpose. This study assessed retinal cells in the macula of human donors with diabetes with or without retinopathy.

Methods. Seventeen human donor retinas were classified as diabetes mellitus (DM, $n = 7$), diabetes with diabetic retinopathy (DR, $n = 3$), or control ($n = 8$). Macular transversal sections were analyzed for photoreceptors, bipolar cells, horizontal cells, ganglion cells, their synaptic connections, and Müller cells using immunohistochemistry and confocal microscopy. The densities of bipolar cells, horizontal cells, and ganglion cells and the thickness of the inner plexiform layer (IPL) were quantified around the fovea.

Results. In the macula, cone photoreceptors elongated their axons to establish synapses with bipolar and horizontal cells in intraretinal cysts. Bipolar cells were reduced in the DM group compared to the control ($P < 0.001$), and rod bipolar cells showed morphological alterations in the cell body and synaptic terminals in both diabetic groups. Morphological changes were observed in both plexiform layers, with a decrease in the IPL thickness in DR. Horizontal cell terminals sprouted into the outer and inner retina in DR, despite no density differences existing between DM and control ($P = 0.498$). Ganglion cell density was reduced in the DM retinas compared to control ($P < 0.001$). Müller cells exhibited thickening of their cell bodies and end feet in all diabetic retinas.

Conclusions. The degeneration of neurons and synaptic connectivity within the macula in individuals with DM, even in the absence of clinical vascular signs, is associated with impaired visual function. These early changes suggest potential new biomarkers for imaging techniques and emphasize the need for therapies for diabetic patients without clinical signs.

Keywords: human eyes, retina, diabetes, diabetic retinopathy, ganglion cells, inner nuclear layer, Müller cells, photoreceptor

Diabetes mellitus (DM) is a chronic metabolic disease characterized by elevated blood glucose levels, resulting from defects in insulin secretion by the pancreas (type 1 DM) and/or an impaired cellular response to insulin (type 2 DM).[1] Type 1 DM is an autoimmune disease that typically manifests in childhood,[2] whereas the insulin resistance associated with type 2 DM usually develops after the age of 40 years.[1] Diabetic retinopathy (DR) is the main complication in the retina of both types of diabetes,[3] and it is related to the long-term cell damage caused by the high glucose levels in the bloodstream.[4] Classically, the main cause of vision loss in patients with DR has been attributed to vascular degeneration, without considering the possible neuronal involvement.[3] The stages of the disease are currently based on the microvascular changes and the development of diabetic macular edema.[5]

More recent studies suggest functional or structural alterations through various imaging techniques in diabetic patients without retinopathy,[6,7] and the Diabetic Retinopathy Preferred Practice Pattern considers DR to be a neurovascular disease.[5] Among these signs, diabetic patients without retinopathy presented a reduction in the electroretinographic (ERG) b-wave response.[8] The main structural alterations described in some diabetic patients without retinopathy include loss of the ganglion cell layer (GCL) or retinal nerve fiber layer (RNFL), as determined using optical coherence tomography (OCT) techniques.[6,9] Despite this, most of the research done on the frontline is being conducted in animal models,[10] and the neuronal alterations of human retinas in diabetic patients are still unknown.

Herein, with the aim to contribute to the establishment of the fundamental basis of DR, we studied the morphological alterations of retinal cells in the macula of postmortem eyes from diabetic donors with or without DR diagnosis. The findings from this study will favor the interpretation of the signs observed through imaging techniques such as OCT and

encourage the development of more targeted treatments to slow down the progression of the disease.

Materials and Methods

Research Design and Source of Human Samples

This cross-sectional study compared the retinal histology of human donors with DR (DR group), those with diabetes without retinopathy signs (DM group), and healthy donors (control group). The inclusion criteria for the control group included no retinal diseases or other comorbidities that may lead to retinal alterations, when possible. The inclusion criteria for the study group required participants to be 40 years or older, have a clinical diagnosis of diabetes mellitus and, if present, diabetic retinopathy, and were without any other retinal disease that could act as a confounding factor.

Retinal samples from human donor eyes were also obtained postmortem from the University Hospital of San Juan Alicante. Eyes included in this study were processed for cell biology techniques, whereas contralateral eyes were processed and stored for potential molecular biology analyses in future studies. The procedures involving the use of human tissue were carried out in compliance with the tenets of the Declaration of Helsinki and were approved by the Ethics Committee on Human Research of the University of Alicante (UA-2018-04-17). The informed consent was signed previously by the donor or the donor's family. A total of 18 human eyes were included from 18 donors: eight from control subjects and 10 from patients with DM or DR. The number of retinas used for each analysis depended on the sample condition after processing and the availability of samples.

Tissue Processing and Retinal Immunohistochemistry

Eye enucleation was performed between 1 and 3 hours postmortem, followed immediately by immersion of the eyes in a 4% paraformaldehyde solution for 2 hours at room temperature. Subsequently, the samples were rinsed in 0.1-M phosphate buffer and, after an incision had been made at the corneal limbus, eyes were cryoprotected using sucrose gradients (15%, 20%, and 30%) at 4°C. After the anterior segment of the eye was removed, the posterior pole was dissected into nine segments (Fig. 1a), keeping the fovea and optic nerve on the temporal central portion (Fig. 1b). The temporal 1 portion containing the macula was used to obtain 14-µm transversal sections with the cryostat and to perform immunohistochemical analysis. The anti-

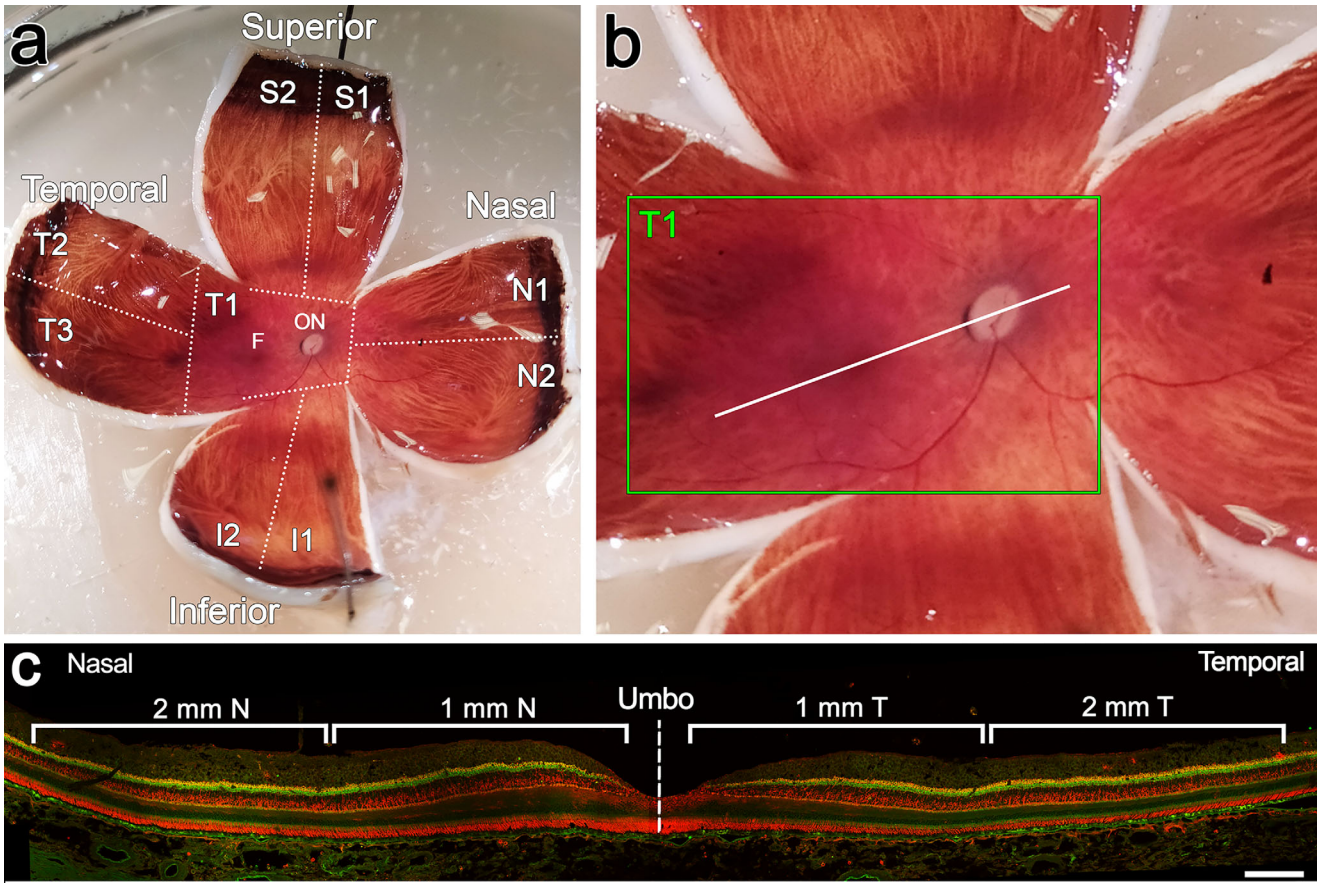

Figure 1. Regions of retinal analysis. (**a**) Ocular globe after dissection into nine segments. (**b**) The analyzed area of the retinal cross-section, including the macula and optic nerve (temporal 1, T1). The *white line* includes the area assessed in the foveal sections. (**c**) The foveal cross-section shows the areas evaluated at different distances from the umbo (*white lines*), where bipolar cell density, horizontal cell density, and IPL thickness were measured. Retinal cross-sections were immunostained with anti-GNB3 (*red*) and anti-Bassoon (*green*) antibodies. *Scale bars*: 200 µm (**c**).

Investigative Ophthalmology & Visual Science

Table 1. Primary and Secondary Antibodies Employed in the Study

Immunogen	Host Species (Class)	Source (Catalog No.)	Dilution
Bassoon	Mouse (M, clone SAP7F407)	Enzo Life Sciences (ADI-VAM-PS003)	1:100
Calbindin	Rabbit (M, clone D-28K)	Swant (CB-38a)	1:500
CRALBP	Mouse (M, clone B2)	Abcam (ab15051)	1:200
GFAP	Mouse (M, clone G-A-5)/ guinea pig (P)	Sigma-Aldrich (G3893), Synaptic Systems (173 004)	1:200
GNB3	Goat (P)	Sigma-Aldrich (SAB2501537)	1:50
Parvalbumin	Rabbit (P)	Swant (PV27)	1:1000
PKCα	Rabbit (P)	Sigma-Aldrich (P4334)	1:500
RBPMS	Rabbit (P)	Merck Millipore (ABN1362)	1:200
VGlut1	Guinea pig (P)	Merck Millipore (AB5905)	1:100
Invitrogen NucRed Dead 647 Ready Probes Reagent (TO-PRO-3 iodide)	—	Thermo Fisher Scientific (R37113)	1:1
Anti-goat conjugated to Alexa Fluor 555	Donkey (P)	Thermo Fisher Scientific (A32816)	1:100
Anti-guinea pig conjugated to Alexa Fluor 633	Donkey (P)	Thermo Fisher Scientific (A21105)	1:100
Anti-mouse conjugated to Alexa Fluor 488	Donkey (P)	Thermo Fisher Scientific (A21201)	1:100
Anti-mouse conjugated to Alexa Fluor 555	Donkey (P)	Thermo Fisher Scientific (A31570)	1:100
Anti-rabbit conjugated to Alexa Fluor 488	Donkey (P)	Thermo Fisher Scientific (A210206)	1:100
Anti-rabbit conjugated to Alexa Fluor 555	Donkey (P)	Thermo Fisher Scientific (A31572)	1:100

M, monoclonal; P, polyclonal.

bodies specifically labeled cones (calbindin), bipolar cells (guanine nucleotide-binding protein subunit beta 3 [GNB3] and protein kinase C alpha [PKCα]), horizontal cells (parvalbumin), all ganglion cells (RNA binding protein with multiple splicing [RBPMS]), presynaptic connections (Bassoon and vesicular glutamate transporter 1 [VGlut1]), the structure of Müller cells (cellular retinaldehyde-binding protein [CRALBP]), and their activation (glial fibrillary acidic protein [GFAP]), as other studies have previously reported.[11–13] Retinal sections were washed three times in phosphate buffer and incubated in 10% donkey serum for 1 hour. The primary antibody (Table 1) diluted in phosphate buffer with 1% Triton X-100 was incubated overnight at room temperature at 4°C. Then, samples were washed in phosphate buffer and incubated with the secondary antibody (Table 1) for 1 hour at room temperature at 4°C. TO-PRO dye (Thermo Fisher Scientific, Waltham, MA, USA) was added for 15 minutes at room temperature for nuclei staining when possible. Finally, the preparations were washed again, mounted using Citifluor mounting solutions (Citifluor, Hatfield, PA, USA), and coverslipped. Images were obtained with a Leica TCS SP8 confocal laser-scanning microscope (Leica Microsystems, Wetzlar, Germany). Contralateral eyes were processed using RNA*later* (Thermo Fisher Scientific) for preservation.

Morphological Assessment of Retinal Structure and Neurons

Retinal structure was described in transversal sections of the macula using anti-GNB3 antibody to examine the outer and inner retina, anti-Bassoon antibody to evaluate the synaptic connectivity, and anti-calbindin antibody to assess cone photoreceptors. The structure of the photoreceptor cells as well as their synaptic terminals (at the outer plexiform layer [OPL] level) were analyzed by at least two retinal researchers in the transversal sections at the macula immunostained with the anti-GNB3 and anti-Bassoon antibodies. Bassoon protein is the main component of the presynaptic ribbon and regulates synapse formation. For assessment of the OPL, the location (inside the terminal, along the axon), distribution (linear structure, diffuse or widespread presence of the protein in the terminal), and uniformity (continuous or discontinuous terminals) of the ribbon were considered. A total of 13 samples were used (control, $n = 6$; DM, $n = 5$; DR, $n = 2$), and only well-oriented areas of the retinal sections were included.

Cellular Quantification of Bipolar and Horizontal Cells and Thickness of the Inner Plexiform Layer

Confocal images of the transversal sections at the foveola were used to assess the number and morphological changes of bipolar and horizontal cells. The thickness of the inner plexiform layer (IPL) was also analyzed. Quantification was performed 1 mm and 2 mm from the foveal umbo on the nasal and temporal sides (starting 100 µm from the center of the umbo) using Photoshop 22.5.4 (Adobe, San Jose, CA, USA) (Fig. 1c).

Two or three complete retinal sections were imaged from each sample in the foveola using the 40× objective. A total of 14 samples were used to quantify the number of the GNB3$^+$ bipolar cells (control, $n = 5$; DM, $n = 7$; DR, $n = 2$), and 13 samples for the parvalbumin$^+$ horizontal cells (control, $n = 5$; DM, $n = 5$; DR, $n = 3$). The structure of rod bipolar cells was assessed using the anti-PKCα antibody, and synaptic connectivity was also evaluated with the anti-VGlut1 antibody. The thickness of the IPL was measured considering the Bassoon immunostaining in 12 samples (control, $n = 5$; DM, $n = 5$; DR, $n = 2$). Within each area, 10 different points separated by 100 µm each were measured.

The results were normalized using different reference parameters depending on the type of measurement. For bipolar and horizontal cells, the data were normalized to the studied area of the retinal section, expressed as cells per square millimeter (cells/mm^2). In contrast, for the IPL, the results were normalized to the total retinal thickness in the areas where the measurements were performed. Both the total retinal area and the total retinal thickness were measured within 1 mm and 2 mm from the center of the retina, extending both nasally and temporally (Fig. 1c).

Investigative Ophthalmology & Visual Science

Morphological Analysis and Quantification of Ganglion Cells

Confocal images of the transversal sections at the foveola were used to assess the number and the morphological changes of ganglion cells with the use of anti-RBPMS and anti-parvalbumin antibodies, respectively. The RBPMS$^+$ ganglion cells with the TO-PRO at the GCL were quantified within 1 mm from the foveal umbo in the nasal (N1, N2) and temporal side (T1, T2) with Adobe Photoshop 22.5.4. The count started from the beginning of the GCL, with each area measuring 500 µm in length. Two or three retinal sections were imaged from each sample in the foveola using the 40× objective. A total of 14 samples were used to quantify the number of the ganglion cells (control, $n = 5$; DM, $n = 7$; DR, $n = 2$).

Assessment of Müller Cells and Reactive Gliosis

Müller cells were evaluated in the foveal sections immunostained with anti-CRALBP (control, $n = 6$; DM, $n = 5$; DR, $n = 2$) and anti-GFAP (control, $n = 5$; DM, $n = 5$; DR, $n = 2$) antibodies and were imaged using the confocal microscope. The structure of the honeycomb-like pattern at the outer nuclear layer (ONL) level, the continuity of the external limiting membrane (ELM), swelling of the cells, and intense immunolabeling at the cell nuclei were considered in the morphological analysis of Müller cells. Reactive gliosis was evaluated according to the immunostaining of GFAP in the cells.

Statistical Analysis

Statistical analysis was conducted using SPSS Statistics 27.0 for Macintosh (IBM Corp., Chicago, IL, USA). The normality of the variables was assessed using the Shapiro–Wilk test, and the homogeneity of variances was evaluated using Levene's test. Two-way ANOVA was performed to assess the differences between groups (control and diabetic) considering the different retinal locations around the fovea. Bonferroni correction was applied for post hoc pairwise comparisons. The Mann–Whitney U test was applied in nonparametric analysis. Graphs were plotted using Prism 9.4.1 (GraphPad Software, Boston, MA, USA), and results were considered statistically significant for $P < 0.05$. Statistical tests were not performed on the DR group due to the small sample size; however, mean values were included in the graphs and tables.

Results

Sample Description

The retinas of the diabetic group were classified based on the clinical data and the presence of vascular sign characteristics of diabetic retinopathy: seven eyes showed no signs of retinopathy (DM group) (Fig. 2b), and three eyes had DR (Figs. 2c, 2d; Table 2). Within the DR group, two retinas exhibited proliferative DR, and photocoagulation spots were found in the mid-periphery. Fibrovascular tissue and hemorrhages were present in the DR-2 sample (Fig. 2d). No significant differences in age were observed among the three groups (control, 60 ± 8 years; DR, 60 ± 8 years; DM, 64 ± 8 years; $P = 0.461$). Arterial hypertension was the predominant comorbidity, present in 50% of the control group and 87.50% in the diabetic group (DR+DM). Demographic data are provided in Table 2.

Disruption of the Foveal Structure

Progressive changes in the macula were observed within different stages of the disease (Fig. 3). The loss of the foveal structure began with the presence of intraretinal cysts (Fig. 3b, asterisks) and continued with macular edema (Fig. 3c). A disorganization of the retinal layers was present in more advanced stages (Fig. 3c). The use of Bassoon to analyze synaptic connectivity within the foveal pit revealed a progression in the disruption of the connectivity throughout the disease (Figs. 3b', 3c'). Bassoon protein is found in the synaptic ribbon of the presynaptic terminal in cone and rod photoreceptors and bipolar cell axons. Compared with the control, an impairment of the synapses in both plexiform layers at the foveola was already found in a diabetic retina without DR (Fig. 3a' vs. Fig. 3b'). In retinas with DR, these layers were almost absent and completely unstructured in the foveola (Fig. 3c').

Structural Impairment of Photoreceptors and Changes in Synaptic Connectivity in the Diabetic Retinas With and Without DR

In retinas with DR at the perifovea, cones undergo pronounced morphological and synaptic alterations compared to controls (Fig. 4). Immunostaining with anti-calbindin antibodies revealed significant disorganization of cone structures, including disruption of the orderly arrangement of cone cell bodies and their external and internal segments. Cone axons appeared distorted, losing their typical uniform and parallel alignment, and their pedicles exhibited aberrant morphologies, deviating from the upright structure observed in the controls (Fig. 4b vs. Fig. 4a). Specifically, the normal morphology of cone pedicles and the linear arrangement of Bassoon immunoreactivity in the control group differed from the impaired cone pedicle morphology and disrupted synaptic ribbons in the DR sample (Fig. 4a' vs. Fig. 4b', arrowheads). Double immunostaining with Bassoon highlighted a disruption of the OPL, characterized by a loss of synaptic ribbons at cone synaptic contacts with horizontal and bipolar cells (Figs. 4b, 4b' vs. Figs. 4a, 4a'). In the fovea of DR, these alterations were more severe. Pedicles were difficult to identify, and extensive cone disorganization existed (Figs. 4c, 4c' vs. Figs. 4a, 4a'). Furthermore, only a few Bassoon-immunoreactive puncta, corresponding to rod axon terminals, remained detectable in these advanced stages (Figs. 4c, 4c').

Additionally, the synaptic connectivity in both plexiform layers was assessed in the well-oriented retinal cross-sections at the foveola and perifovea immunostained with anti-Bassoon antibody. At the OPL, in control retinas close to the foveal pit, the Bassoon formed a continuous line concentrated at the edge of the cone pedicle (Fig. 5a, arrowheads). This typical distribution was present in 40% of control retinas and 20% of DM retinas. Although 60% of the control retinas also exhibited diffuse Bassoon localization across the pedicle, a higher percentage of DM retinas displayed these alterations (80%). Importantly, within this 80% of retinas affected by DM, 75% exhibited either a loss (Fig. 5b) or abnormal accumulation

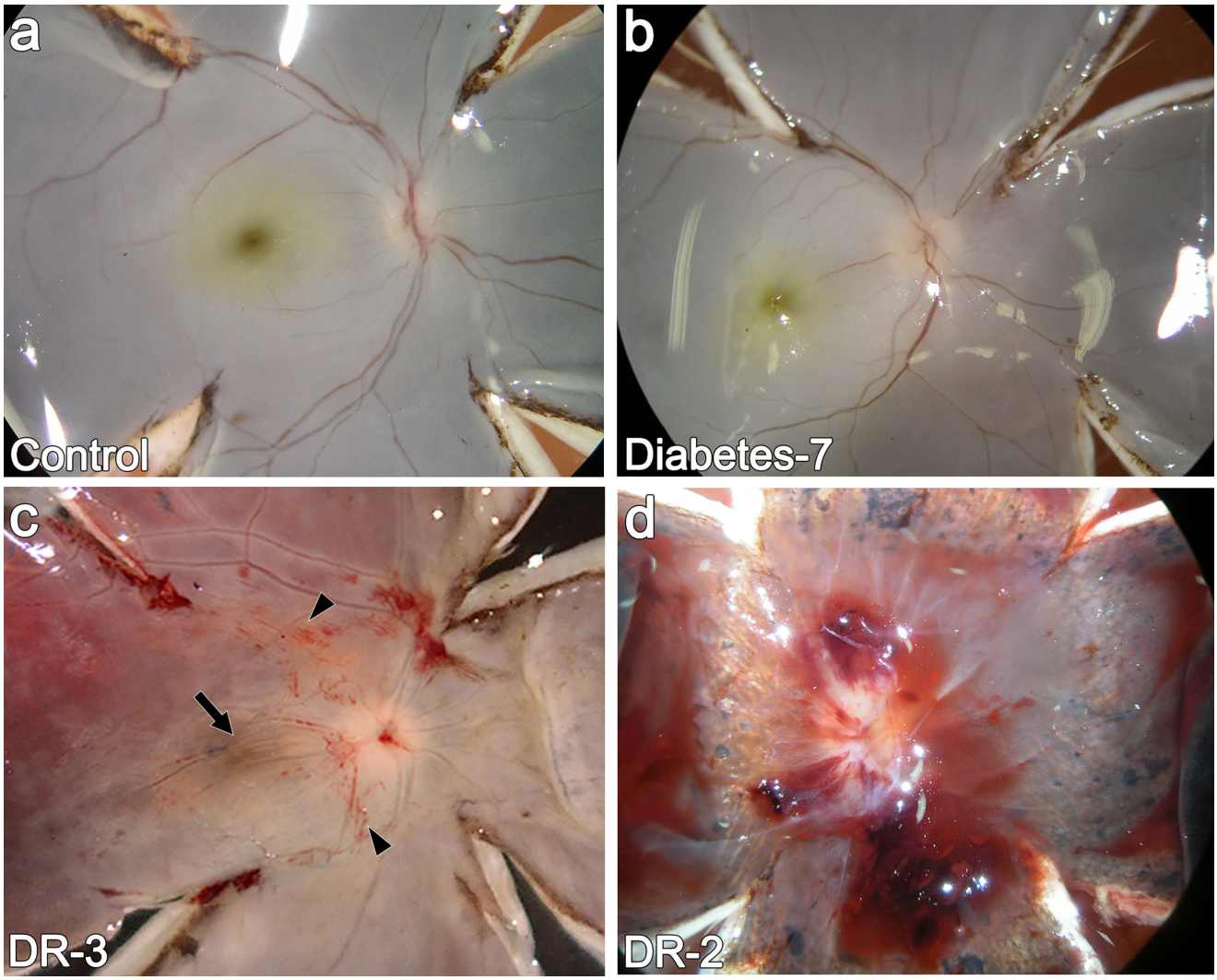

Figure 2. Visualization of the retina after processing. Eyes were treated with RNA*later* for preservation, which changed the appearance of the translucent retina to *white*. (**a**, **b**) Normal distribution of the retinal vessels observed in control and diabetic retinas. (**c**) Flame and dot hemorrhages, mainly at the vascular arcades, and retinal tractions at the macula were present in DR-3. (**d**) Fibrovascular tissue and hemorrhages around the optic nerve were present in a case of proliferative DR (DR-2).

Table 2. Clinical Description of the Samples

Subject	Experimental Group	Age (y)	Sex	Ocular Pathologies	Comorbidities
C-1	Control	72	F	None	Arterial hypertension
C-3	Control	74	M	None	Arterial hypertension, auricular fibrillation, hyperuricemia
C-5	Control	74	M	None	Arterial hypertension
C-13	Control	57	F	None	Arterial hypertension
C-14	Control	65	M	None	None
C-15	Control	62	M	None	None
C-16	Control	60	M	None	None
C-17	Control	54	F	None	None
DR-1	DR	66	M	DR	DM, arterial hypertension, chronic kidney disease
DR-2	DR	40	M	Proliferative DR	DM, arterial hypertension
DR-3	DR	56	M	Proliferative DR	DM, arterial hypertension
D-4	DM	65	F	Surgically repaired retinal detachment	DM, arterial hypertension, hyperthyroidism
D-5	DM	68	M	None	DM, arterial hypertension
D-6	DM	61	M	None	DM, ischemic cardiomyopathy
D-7	DM	56	M	None	DM, arterial hypertension
D-8	DM	79	M	None	DM, arterial hypertension, dyslipidemia, atrial fibrillation
D-9	DM	61	M	None	DM
D-10	DM	56	F	None	DM

F, female; M, male.

Investigative Ophthalmology & Visual Science

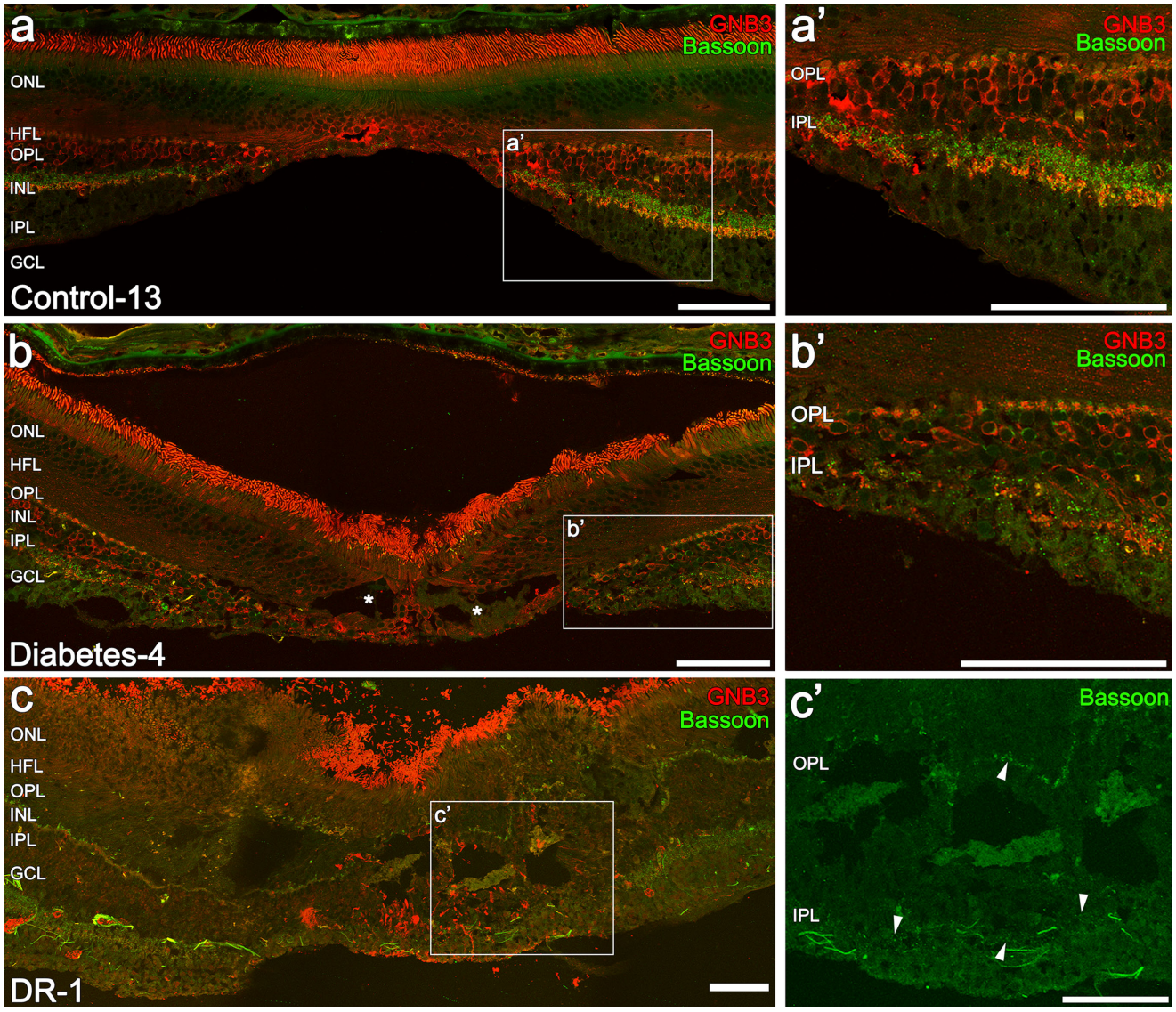

Figure 3. Fovea of control and diabetic samples without and with diabetic retinopathy. Photoreceptors and ON bipolar cells were immunostained with anti-GNB3 antibody (*red*), and the OPL and IPL were labeled with anti-Bassoon antibody (*green*). (**a'–c'**) Magnification insets showing plexiform layers: (**a**, **a'**) Fovea from a control donor showing exclusively the photoreceptors at the umbo, and the appearance of the rest of the retinal layers afterward. (**b**, **b'**) Fovea from a diabetic patient with intraretinal cysts in the ONL at the umbo (*) and alterations in the plexiform layers. (**c**, **c'**) Thickening and disorganization of the retinal layers at the fovea in the DR-1 retina. *Scale bars*: 100 µm. Please note that the scale differs between images to show the entire fovea, but the retina area in **c** is larger than in **a** and **b**.

(Fig. 5c) of Bassoon. Finally, all DR retinas exhibited either a complete loss of the protein or an abnormal accumulation of Bassoon throughout the pedicle (Fig. 5d, arrowheads). None of these alterations was observed in the control retinas.

Otherwise, in some regions of the IPL in the DM and DR groups, there was either a loss of immunoreactive dots and disorganization of the Bassoon or a complete absence of the protein (Figs. 5b'–5d' vs. Fig. 5a'). The thickness of the IPL showed no changes between control and DM retinas in the fovea (Fig. 5e). However, the IPL was significantly thinner in regions close to the foveal pit in the DR group compared to control and DM retinas (Fig. 5e, Table 3). The IPL was not distinguished in the more peripheral regions of the DR group (Supplementary Fig. S1, Supplementary Table S1).

Photoreceptor Structure in Response to Intraretinal Cysts

Most intraretinal cysts were found in the Henle fiber layer (HFL) (Figs. 3b, 3c; Figs. 6b–6f). Forty percent of the DM retinas (2/5, D-4 and D-8) and both of the DR retinas (2/2) analyzed showed intraretinal cysts at the HFL (Fig. 6). Moreover, although the synaptic connectivity was altered in DM retinas with the cysts, photoreceptors preserved the rest of their morphology (Fig. 6b). Photoreceptors in DR retinas with cysts showed different degrees of atrophy (Figs. 6c, 6d). Most cysts contained accumulated material and lacked the vascular wall.

In advanced stages of proliferative DR with intraretinal cysts, cone photoreceptors expand their axons, trying to preserve the synapses with the bipolar and horizontal cells

Investigative Ophthalmology & Visual Science

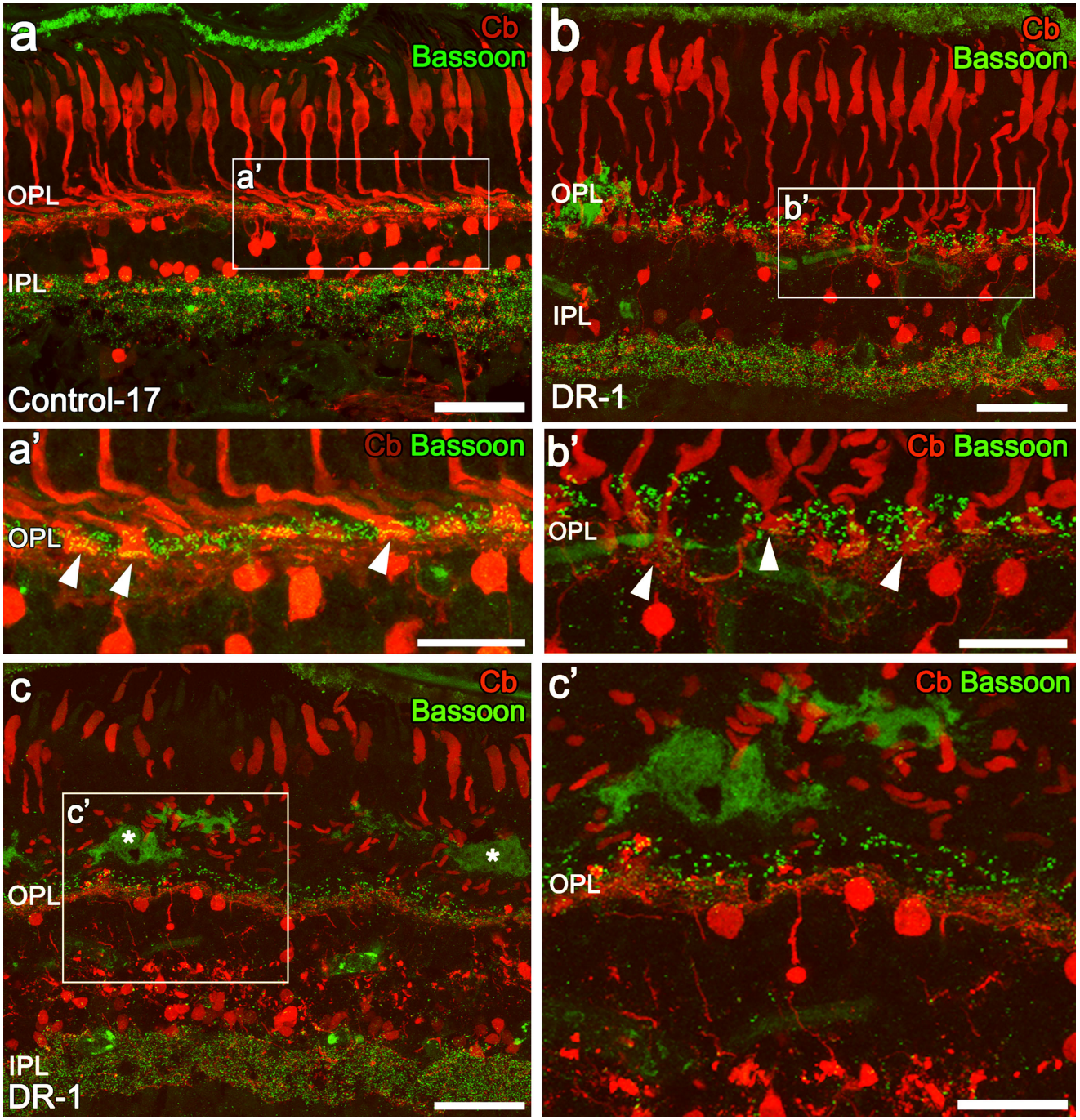

Figure 4. Cone morphology and synaptic connectivity at the OPL in the parafovea and perifovea. (**a**) Structure of cone photoreceptor (calbindin, *red*) and Bassoon antibody distribution (*green*) in the plexiform layers in an age-matched control. (**b**) Disruption of cone structure and synaptic connectivity, with aberrant pedicles, in a retina with DR at the perifovea. (**c**) Extensive degeneration of cones and synaptic connectivity in DR at the parafovea. (**a'–c'**) High-magnification images of the cone pedicles and Bassoon antibody distribution in control retina (**a'**, *arrowheads*) and one retina with DR at different eccentricities from the fovea (**b'**, **c'**, *arrowheads*). *Small green dots* outside the pedicles correspond to rod axon terminals. *Intraretinal cysts. *Scale bars*: 50 µm (**a–c**); 25 µm (**a'–c'**).

(Figs. 6e, 6f, arrowheads), causing the disappearance of the typical structure of the HFL. Specifically, in the DR-1 retina, the pedicles exhibited a smaller and more spherical structure and the synaptic ribbon (immunostained with anti-Bassoon) was concentrated in one cluster (Fig. 6e, arrow) compared with the morphology of the synaptic terminal in the control retina (Figs. 4a, 4a').

Second-Order Neurons: Degeneration of Bipolar Cells and Sprouting of Horizontal Cells in the Diabetic Retinas

The bipolar cells were evaluated in several areas of the transversal sections of the fovea immunostained with anti-GNB3 and anti-PKCα antibodies. The GNB3 protein is

Investigative Ophthalmology & Visual Science

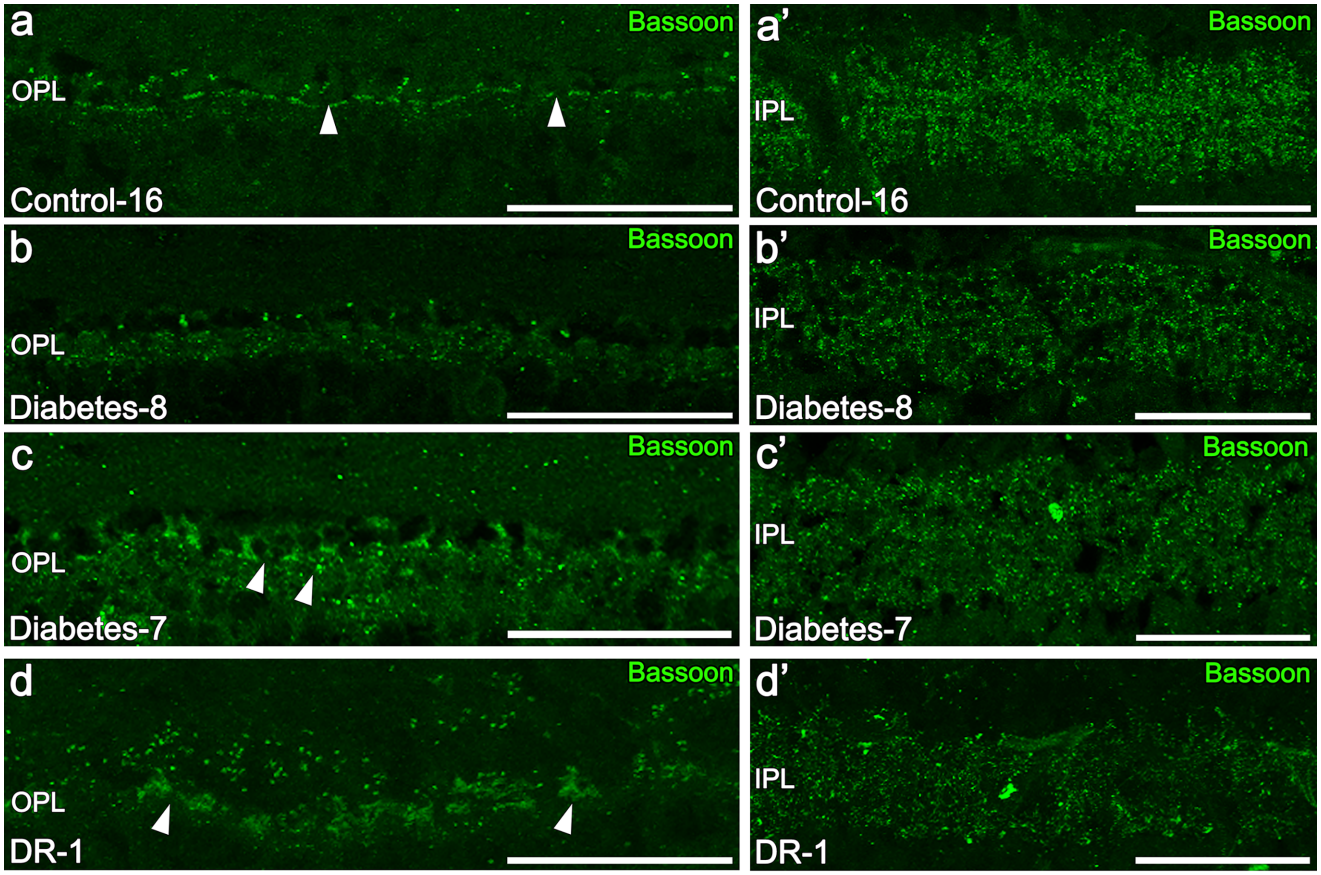

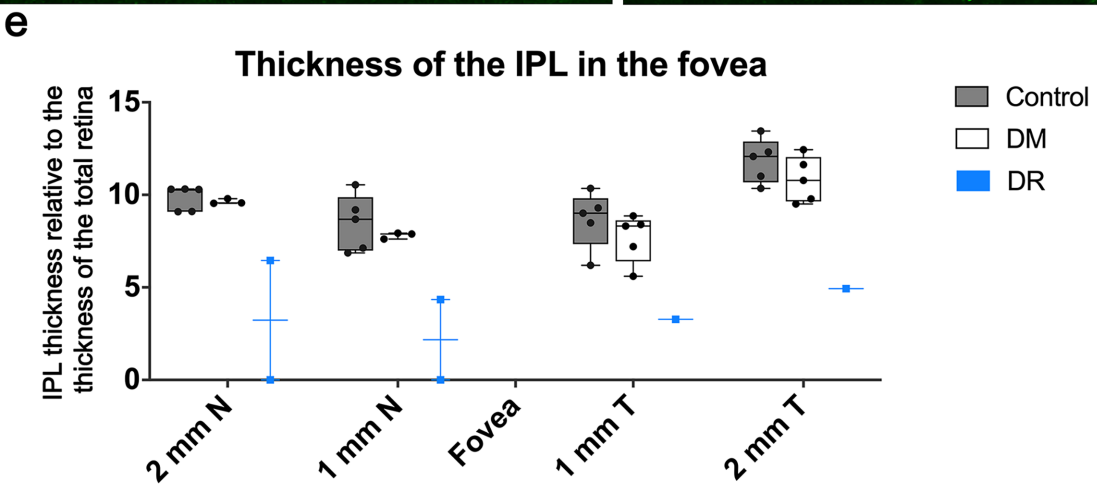

Figure 5. Outer and inner plexiform layers in the fovea of control and diabetic patients. Shown are magnifications of the OPL and IPL next to the foveal depression (nasal in **a**–**c**, temporal in **d**) immunostained with anti-Bassoon antibody. (**a**, **a'**) Characteristic distribution of Bassoon in the OPL (**a**, *arrowheads*) and IPL (**a'**) in control retina. (**b**) A decrease and disorganization of the Bassoon protein in the OPL appeared in some diabetic patients. (**c**, **d**) Accumulation of the same protein in the cone pedicles was present in other samples with diabetes or DR (*arrowheads*). Compared with the control retinas (**a'**), variations in the Bassoon pattern in the IPL were also found in diabetic retinas without (**b'**, **c'**) or with DR (**d'**). (**e**) No differences existed between control retinas ($n = 5$) and DM retinas ($n = 5$), based on Mann–Whitney *U* tests. The IPL decreased in the DR group. N, nasal; T, temporal. *Scale bars*: 50 µm.

present in both ON cone and ON rod bipolar cells (Fig. 7). There were regions nasal to the foveal lacking GNB3$^+$ bipolar cells in some retinas from the DM group (Fig. 7b) and the DR group (Fig. 7c). In fact, the density of bipolar cells was significantly decreased in the DM group compared with the control ($P < 0.001$) (Fig. 7d, Table 3). This degeneration was more pronounced in the nasal area close to the optic nerve (2 mm nasal; $P < 0.05$) and temporal to the fovea (1 mm temporal; $P < 0.01$) compared with the control group (Fig. 7d). The mean densities of bipolar cells in the DR group were lower than in the other groups in most areas (Table 3). No differences were observed in the density of bipolar cells in more peripheral areas in the DM group compared to the control ($P = 0.078$) (Supplementary Table S1, Supplementary Fig. S2).

Table 3. IPL Thickness and Density of GNB3$^+$ Bipolar Cells, Parvalbumin$^+$ Horizontal Cells, and RBPMS$^+$ Ganglion Cells

		Experimental Groups			
Parameter	**Location**	**Control**	**Diabetes Mellitus**	**Diabetic Retinopathy**	***P***
IPL thickness, Bassoon (µm)	2 mm nasal	9.8 ± 0.3	9.6 ± 0.08	3.22 ± 3.22	0.655
	1 mm nasal	8.48 ± 0.68	7.8 ± 0.1	2.17 ± 2.17	0.655
	1 mm temporal	8.66 ± 0.68	7.67 ± 0.58	3.28	0.117
	2 mm temporal	11.8 ± 0.53	10.83 ± 0.55	4.92	0.251
GNB3$^+$ bipolar cells (n°/mm^2)	2 mm nasal	670 ± 30	510 ± 60	100 ± 100	<0.001*
	1 mm nasal	570 ± 30	440 ± 70	330 ± 80	
	1 mm temporal	630 ± 50	380 ±30	370 ± 40	
	2 mm temporal	730 ± 40	580 ± 50	390 ± 50	
Parvalbumin$^+$ horizontal cells (n°/mm^2)	2 mm nasal	290 ± 20	290 ± 20	130 ± 60	0.498*
	1 mm nasal	380 ± 10	360 ± 7	170 ± 80	
	1 mm temporal	380 ± 10	370 ± 15	160 ± 60	
	2 mm temporal	330 ± 20	330 ± 10	150 ± 50	
RBPMS$^+$ ganglion cells (n°/mm^2)	N2	1350 ± 110	920 ± 70	220 ± 200	<0.001*
	N1	1050 ± 80	760 ± 70	200 ± 190	
	T1	1110 ± 80	770 ± 30	140 ± 120	
	T2	1350 ± 110	1080 ± 100	270 ± 210	

The nasal and temporal distances are defined with respect to the foveal pit. Sample sizes: Bassoon$^+$ IPL thickness (control, $n = 5$, DM, $n = 5$, DR, $n = 2$); GNB3$^+$ bipolar cells (control, $n = 5$, DM, $n = 7$, DR, $n = 2$); parvalbumin$^+$ horizontal cells (control, $n = 5$, DM, $n = 5$, DR, $n = 3$); and RBPMS$^+$ ganglion cells (control, $n = 5$, DM, $n = 7$, DR, $n = 2$). The Mann–Whitney *U* test results are shown for the control and DM groups for IPL thickness.

N1 and N2 represent: the first 500 µm from the umbo (N1), and the next 500 µm following N1 (N2) towards the nasal side. Same for T1 and T2 toward the temporal side.

* Two-way ANOVA results for bipolar, horizontal, and ganglion cell quantification, including control and DM groups.

The main morphological differences in the PKC$^+$ rod bipolar cells appear close to the fovea (Figs. 7e–7g). In control retinas, these cells typically exhibit an oval cell body and a continuous axon that synapses at the ON strata of the IPL (Fig. 7e). In the diabetic group, they tend to present a rounder cell body, areas of cellular material accumulated tortuous along the axon, lack of ramifications in the axon terminal, and loss of synaptic connectivity in the outer strata (Fig. 7f). Remarkably, within the DR group, the PKCα protein was absent in most areas of the retina, and the location of the synaptic strata could not be differentiated using this protein due to the extensive degeneration of the tissue (Fig. 7g, arrow).

The horizontal cells were assessed with the parvalbumin immunostaining in the transversal section of the fovea (Fig. 8). Synaptic connectivity, assessed using the VGlut1 antibody, was also observed (Figs. 6a–6c). Horizontal cells were arranged side by side or surrounding the small vessels of the deep capillary plexus, and their ramifications were in contact with the synaptic terminals of the photoreceptors at the OPL (Fig. 8a). Some diabetic and DR retinas lost their lineal structure and formed clusters (Figs. 8b, 8c, arrowheads); consequently, these clusters resulted in areas devoid of horizontal cell bodies (Figs. 8b, 8c, arrows). Degenerative changes and loss of the immunostaining pattern of the synaptic connectivity were detected using the VGlut1 antibody in the DM and DR retinas compared to the control (Figs. 8b, 8c vs. Fig. 8a, green). In addition, sprouting of the synaptic terminals was observed, as they exhibited long (Figs. 8d, 8e, 8g) or short (Fig. 8f) extensions toward the ONL and, occasionally, toward the INL in the DR retinas (2/2) and also in some DM retinas (2/4) (Figs. 8c–8f). Despite the different levels of retinal degeneration in the DR group, the mean density of the horizontal cells in DR was also inferior to that of the control or DM retinas. The DR-1 retina, at the proliferative stage and with extraretinal tissue, showed the lowest density of horizontal cells (33.55 ± 16.48 cells/mm^2). No differences in the density of the horizontal cells in the fovea were found between the control and DM groups ($P = 0.498$) (Fig. 8g, Table 3) or in the periphery ($P = 0.555$) (Supplementary Table S1, Supplementary Fig. S3).

Third-Order Neurons: Analysis of Ganglion Cells

The RBPMS protein is present in all types of ganglion cells (Figs. 9a–9e). The density of ganglion cells was significantly reduced in the DM retinas compared to the control group in all retinal areas ($P < 0.001$) (Fig. 9e, Table 3). A reduction in the ganglion cells was also observed in the DR group compared with the control and DM groups in all retinal areas (Figs. 9d, 9e; Table 3). Parvalbumin immunostaining was used to assess the structure of the GCL (Figs. 9f–9h). Alterations in the immunostaining of ganglion cells, characterized by areas lacking parvalbumin, were observed in both DM and DR retinas compared to control (Figs. 9g, 9h vs. Fig. 9f). Moreover, parvalbumin was mainly concentrated in the cell body in control samples (Fig. 9f) and the D-7 diabetic retina, whereas other diabetic retinas exhibited denser labeling in the dendrites and axons (Figs. 9g, 9h).

Müller Cells in Fovea From Diabetic Patients

The structure of Müller cells was analyzed in the foveal sections immunostained with anti-CRALBP (Fig. 10). The honeycomb-like pattern and the ELM were preserved in 83.3% of control retinas (5/6), 80% of DM retinas (4/5), and 50% of DR retinas (1/2). Alterations in the ELM were observed in one control retina. The DM retina exhibited strongly stained columns at the ONL with isolated disruptions at the ELM, whereas the DR retina was unstructured.

Investigative Ophthalmology & Visual Science

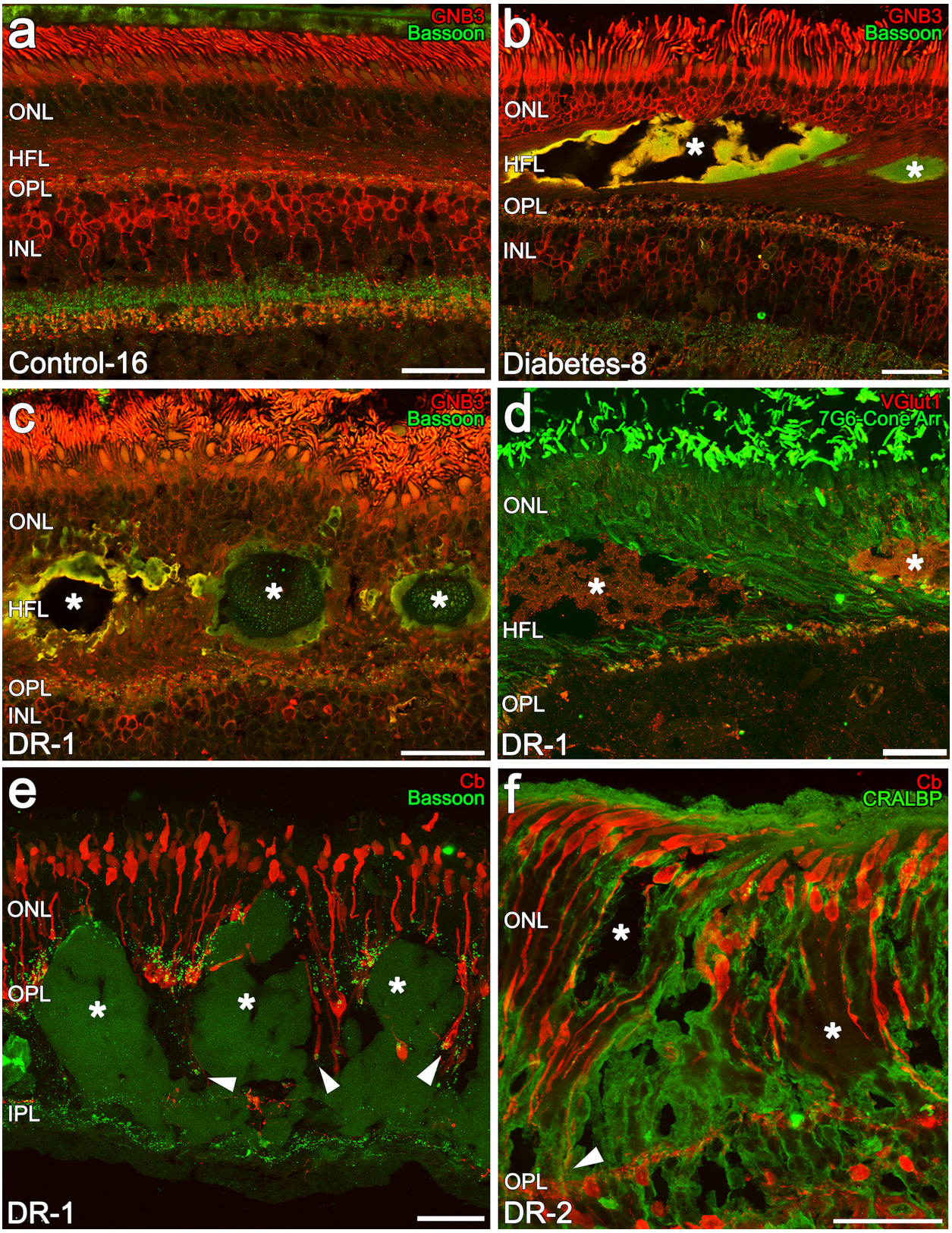

Figure 6. Changes in retinal structure in the presence of intraretinal cysts. Several antibodies were used to assess the photoreceptor and the synaptic connectivity (anti-calbindin, anti- Bassoon, anti-CRALBP, anti-GNB3, anti-7G6 cone arrestin). (**a**) Normal distribution of photoreceptor and synaptic connectivity. (**b**) Different intraretinal cysts at the Henle fiber layer (*) in diabetic retinas. (**c**, **d**) The general structure of photoreceptors was disrupted or atrophic in DR retinas with the cysts. (**e**, **f**) Photoreceptors expanded their axons to maintain synapses with the bipolar and horizontal cells (*arrowheads*). Areas next to the foveal slope are shown: temporal (**a**, **d**), nasal (**b**, **c**), and within the macula (**e**, **f**). *Scale bars*: 50 µm.

Investigative Ophthalmology & Visual Science

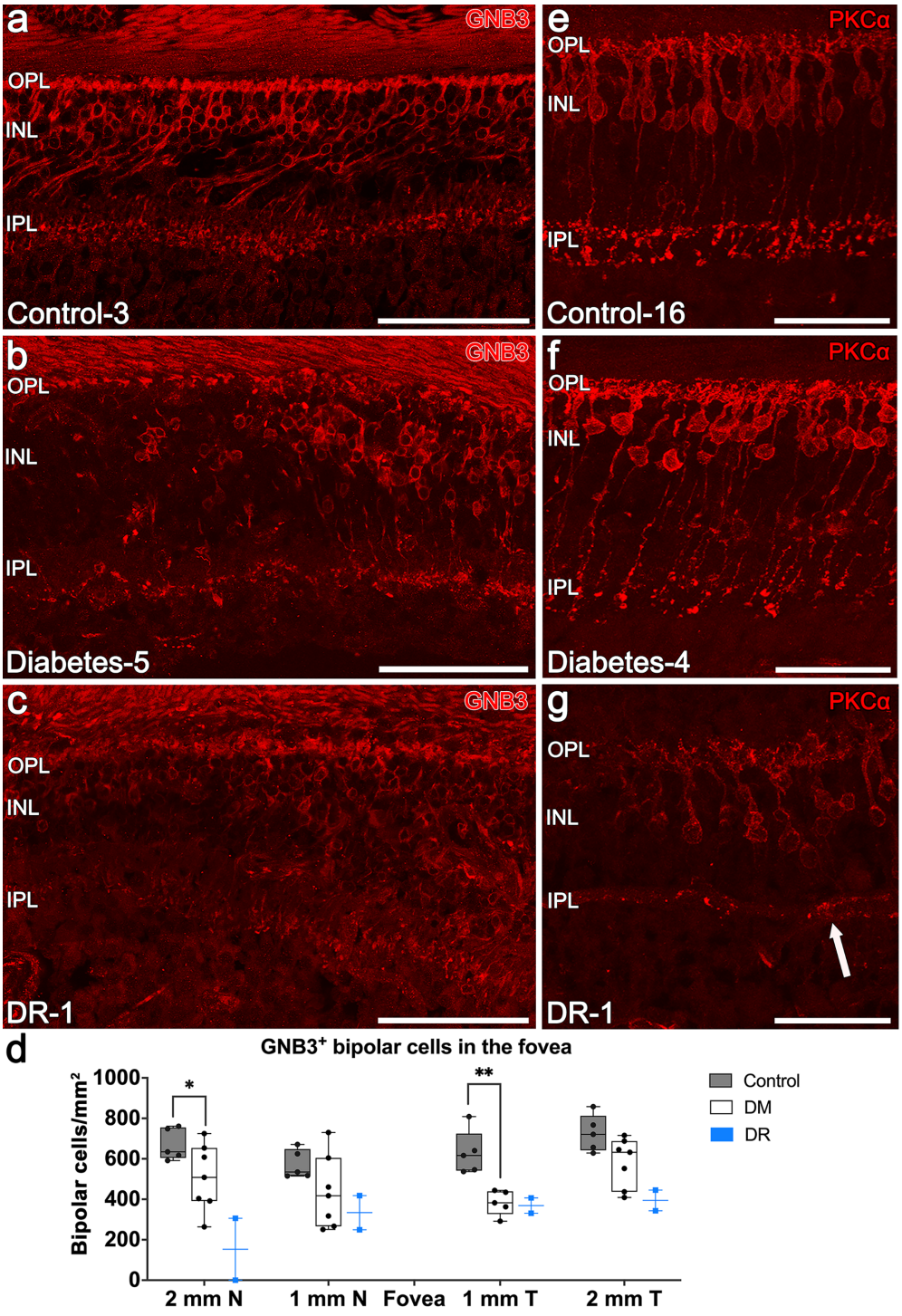

Figure 7. Bipolar cells next to the foveola in control retinas (**a**, **e**) and diabetic retinas without DR (**b**, **f**) and with DR (**c**, **g**). (**a**) Normal pattern of GNB3 immunostaining in a control retina, nasal to the foveal depression. (**b**, **c**) Degeneration and absence of bipolar cells and their synaptic connectivity at the IPL in nasal regions to the fovea in DM retinas (**b**) and DR retinas (**c**). (**d**) Density of bipolar cells at different eccentricities from the fovea in control retinas ($n = 5$) and diabetic retinas without DR ($n = 7$) ($P < 0.001$, two-way ANOVA) and with DR ($n = 2$). (**e**) Bipolar cells from control retina presented an oval cell body with continuous axons and synapses at the ON strata of the IPL. Synaptic connectivity was preserved. (**f**) Bipolar cells from the DM group showed a rounder cell body, accumulation of cellular material along the axon, and loss of connectivity. Synaptic terminals were swollen at the IPL (*arrowheads*). (**g**) Absence of PKCα in most bipolar cells of the DR-1 retina, probably due to retinal degeneration. *Scale bars*: 100 µm (**a**–**c**); 50 µm (**e**–**g**).

The cell body of these cells showed greater immunostaining in most DM retinas (80%, 4/5) compared to controls (50%, 3/6) (Figs. 10b, 10c vs. Fig. 10a, insets). Swollen cell bodies of Müller cells at the foveal depression were one of the main alterations, as they were present in 60% (3/5) of DM retinas and 33.3% (2/6) of control retinas. This swelling,

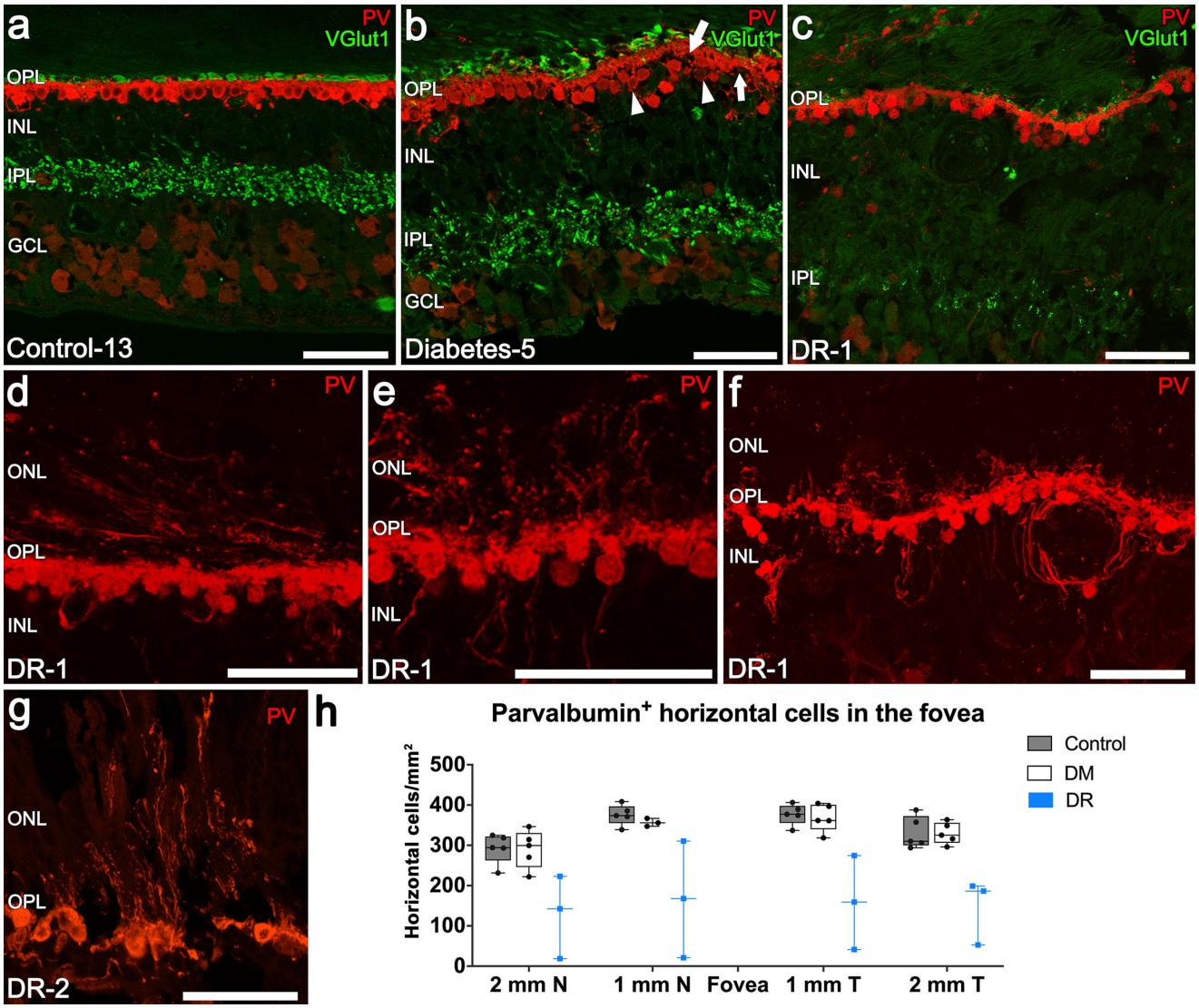

Figure 8. Features of horizontal cells in control and diabetic retinas without and with DR. Retinal cross-sections immunostained with anti-parvalbumin (*red*) and anti-VGlut1 antibodies (*green*). (**a**) Typical distribution of the VGlut1 in the plexiform layers and the horizontal cells arranged side by side, in a control retina. (**b**) In the diabetic retina, these cells lost their lineal structure and formed clusters (*arrowheads*), leading to areas without horizontal cell bodies (*arrows*). (**c**) Loss and disorganization of the horizontal cells and impairment of the synaptic connectivity in diabetic retinopathy. (**d**–**g**) Sprouting or invasion of the ramifications of horizontal cells toward the ONL and INL. (**h**) Density of horizontal cells at different eccentricities from the fovea in control retinas ($n = 5$) and diabetic retinas without DR ($n = 5$) ($P < 0.001$, two-way ANOVA) and with DR ($n = 3$). Areas next to the foveal slope are shown: temporal (**a**, **c**–**e**) and nasal (**b**, **f**, **g**). *Scale bars*: 50 µm.

characterized by a thicker cell body and main process, was predominantly observed in the Müller cells of the foveal pit. One retina from the DR group showed swelling of all of the Müller cells (Fig. 10c), but this swelling could not be distinguished in the other DR retina due to the level of degeneration. In general, swelling in the Müller cell INL was the main characteristic in the DM and DR groups.

Reactive gliosis was evaluated at the fovea by GFAP immunostaining in the Müller cells (Figs. 10d–10g). Sixty percent of control retinas (3/5) and 71.43% of the diabetic retinas (both DM and DR groups, 5/7) showed some level of gliosis. GFAP immunostaining in the Müller cells present in the control retinas was visualized from the end-feet up to the INL. However, within the diabetic retinas, the structure of the Müller cells was either partially GFAP positive (D-7) (Figs. 10e, 10e') or entirely GFAP positive (D-6 and DR-2) (Figs. 10f, 10f', 10g, 10g'). Two samples from the DM group (D-5 and D-6) with reactive gliosis also showed swelling in the INL at the umbo, whereas the other two (D-7 and D-8) presented gliosis without structural alterations in Müller cells. In the DR group, one retina did not show GFAP$^+$ Müller cells, but these cells were completely swollen (DR-1) and the other presented total reactive gliosis and unstructured Müller cells (DR-2) (Fig. 10g').

Discussion

To our knowledge, this study represents the first comprehensive analysis of neural and glial cells alterations in the retina of diabetic donors with or without diabetic retinopathy. To date, functional and imaging tests have primarily been used

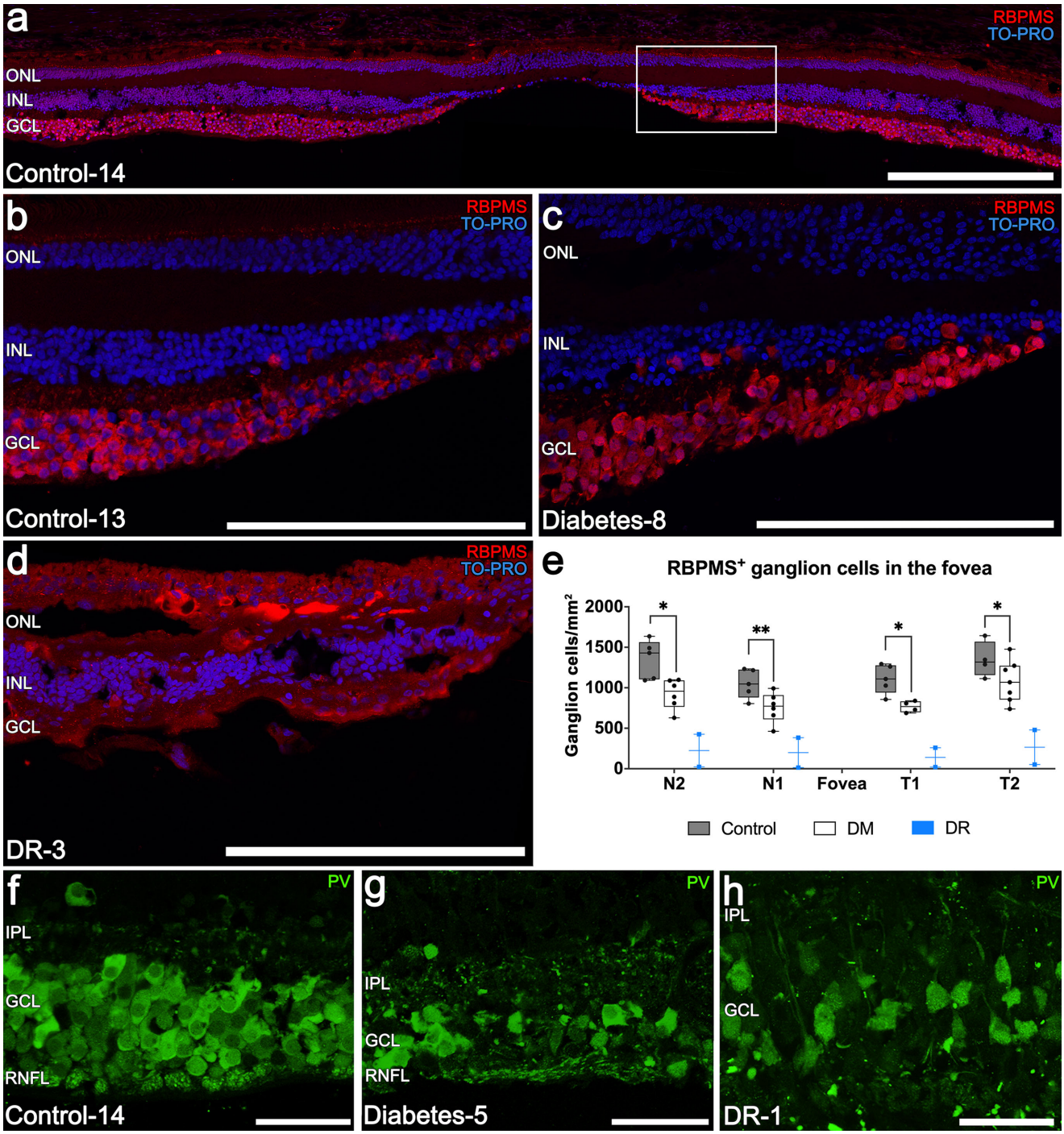

Figure 9. Ganglion cells in the fovea of control and diabetic retinas without and with DR. Shown are retinal cross-sections immunostained with anti-RBPMS and anti-parvalbumin antibodies. (**a**) Foveal section at the umbo from a control retina. (**b–d**) Ganglion cells on the foveal slope in control (**b**), DM (**c**), and DR (**d**) retinas. (**e**) Density of ganglion cells at different locations from the fovea in control retinas ($n = 5$) and diabetic retinas without DR ($n = 7$) ($P < 0.001$, two-way ANOVA) and with DR ($n = 2$). (**f**) Dense immunostaining in the GCL in the control retina. (**g**, **h**) Areas devoid of ganglion cells were observed in diabetic and DR retinas. In most degenerated retinas, parvalbumin was also concentrated in the dendrites of IPL (**g**) and the axons of the RNFL (**h**). Areas next to the foveal slope are shown: temporal (**b**, **d**, **f**, **h**) and nasal (**c**, **g**). PV, parvalbumin. *Scale bars*: 50 µm.

for the evaluation of retinas from diabetic patients,[6,7] in addition to the use of diabetic animal models.[14] Herein, we have provided the first evidence of degenerative histological changes in the fovea of diabetic patients, even in the absence of vascular signs. We focused on the fovea, as it is the most specialized region of the retina, allowing for maximum visual acuity.[12,13] Specifically, a loss of synaptic connectivity along with a reduction of bipolar and ganglion cells, was found in both diabetic groups. Moreover, the sprouting of horizontal cells indicated retinal degeneration, and

Investigative Ophthalmology & Visual Science

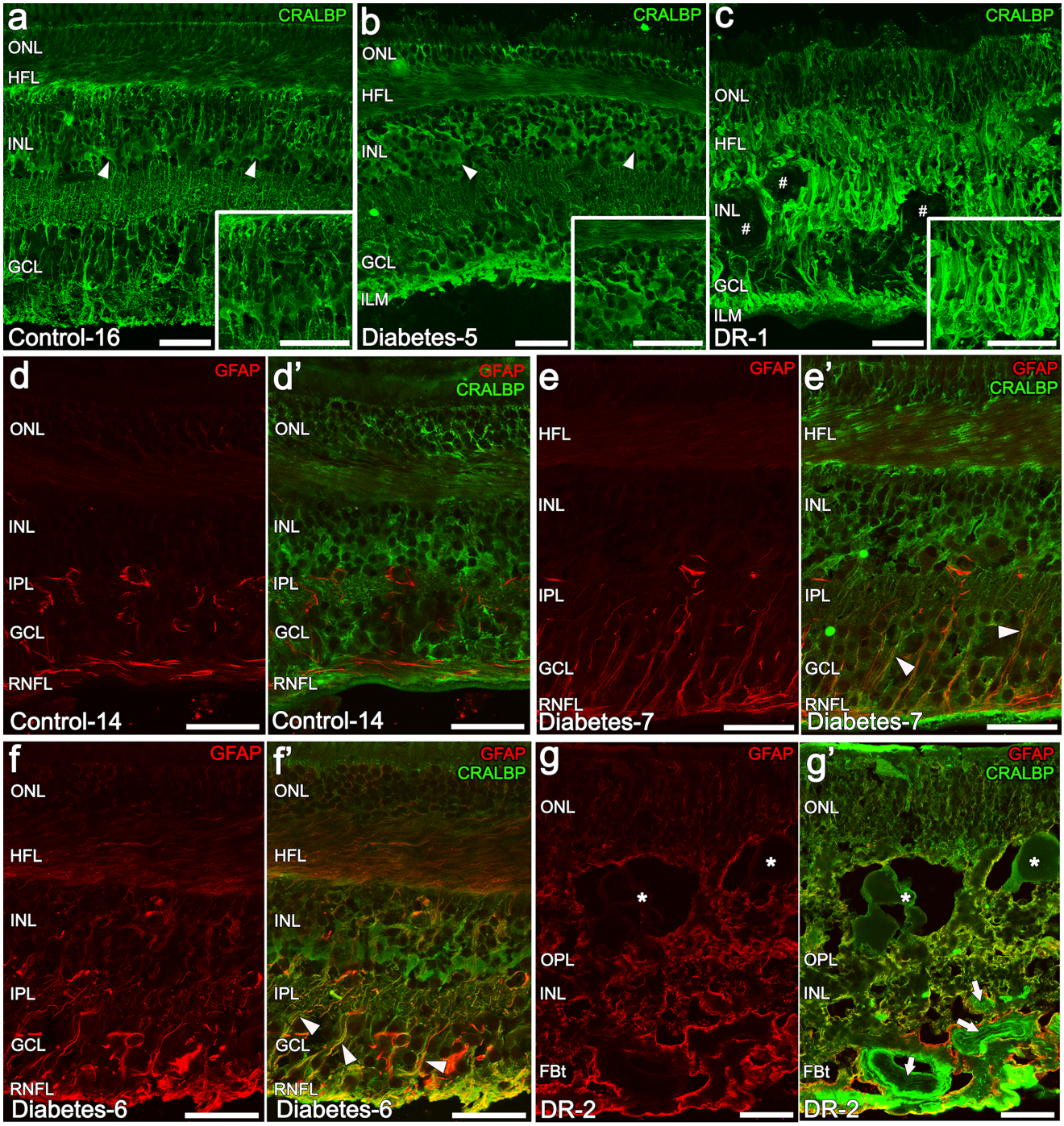

Figure 10. Müller cell structure and reactive gliosis in the parafovea of control and diabetic retinas without and with DR. (**a**) Normal structure of Müller cells in control retina. (**b**) Müller cells showing thickened cell bodies and end-feet (*arrowheads*) in the diabetic retinas without DR. (**c**) Complete swelling of Müller cells in DR. The *lower right insets* in **a** to **c** show high magnification of the Müller cell bodies. (**d**, **d'**) Control retina without reactive gliosis. GFAP was only present in astrocytes. (**e**, **e'**, **f**, **f'**) Different levels of reactive gliosis of Müller cells in diabetic retinas without retinopathy (*arrowheads*). This gliosis was accompanied by thickening of the cell body in some diabetic retinas (**e'**, **f'**). (**g**, **g'**) Anti-GFAP antibody stained the complete structure of Müller cells in the proliferative DR retina (DR-2). Large intraretinal cysts (*) and vessels (**g'**, *arrows*) can be observed. Areas next to the foveal slope are shown: nasal (**a**–**d**, **g**), and temporal (**e**, **f**). FBt, fibrovascular tissue. *Scale bars*: 50 µm.

the activation of Müller cells demonstrated the inflammatory component in these patients.

The disruptions observed at the OPL in our retinas from diabetic donors without vascular alterations may indicate initial degeneration of photoreceptor cells preceding vascular impairment, as described in the cerebral tissue of diabetic rats.[15] The loss of presynaptic proteins,[16–18] including the Bassoon protein that we analyzed, can lead to bipolar cell degeneration and the sprouting of horizontal cell processes into the ONL and INL observed in both diabetic

Investigative Ophthalmology & Visual Science

groups. These synaptic alterations could affect the functional response of the bipolar cells[18–20] and can explain the reduction in the ERG b-wave responses in diabetic patients without retinopathy.[8,21] Although most studies on animal models are focused on the onset of ONL degeneration,[22,23] the downregulation of similar presynaptic proteins occurs prior to the cell apoptosis.[19] Degeneration of the OPL is expected to involve mitochondrial impairment, given the critical role of mitochondria in the photoreceptor terminals. Studying this layer could therefore serve as a potential biomarker for assessing the mitochondrial state of the retina[24] in the context of diabetes. Future studies could focus on a deeper exploration of these mitochondria to better understand their role in retinal degeneration associated with diabetes. Therefore, our findings emphasize the importance of studying synaptic connectivity in diabetic patients and suggest that the decrease of visual function in the absence of vascular alterations[25,26] may be related to this degeneration. Indeed, the use of OCT or multifocal ERG has been proposed to identify changes in the function of photoreceptors that could serve as biomarkers for DR.[27–29] Currently, some studies have analyzed the OPL using imaging techniques,[30] but the results should be interpreted with caution because OCT resolution is insufficient to discriminate the OPL from the HFL.

Results regarding degeneration of the INL are controversial in both animal models and humans. Although some authors have observed no differences in the bipolar cells or the INL when compared to control animals,[20,23] others have reported a reduction in thickness within the INL.[22,31] In diabetic patients without DR or with non-proliferative DR, OCT images indicate either an increase[32,33] or a decrease[34,35] of the inner retina. In any case, whether these changes correspond to bipolar cells remains uncertain considering the composition of the INL. It has been proposed that the increase in the INL is related to either extracellular fluid or the intracellular swelling of Müller cells.[32,36] Specifically, the primary changes observed in Müller cells in the DM group in our study were swelling in the cell bodies, thereby supporting the hypothesis that the increase in INL found in OCT studies is due to intracellular swelling of the cell bodies. Our study showed complete swelling or hypertrophy of these cells only in retinas with stages of proliferative DR, a finding that has also been described in later stages of DR in human[37] and animal[14] models. This hypertrophy occurs due to disruptions in aquaporins, resulting in the accumulation of water within the cell and ultimately leading to a dysregulation of homeostasis.[38] However, in our samples, the swelling was not always associated with reactive gliosis, even in the DR group; some DM retinas showed gliosis without Müller cell alterations. All of these signs may indicate that Müller cells are activated to protect the retina[39] in the early stages of diabetes. However, they seem to preserve their structure until advanced stages, probably because Müller cells are more resistant to oxidative damage than neurons.[40] This resistance is attributed to their glycogen energy reserve, high concentration of antioxidants, and ability to regenerate and ingest excess glutamate toxic to neurons.[40,41]

Our results confirmed the neuronal degeneration of ganglion cells in the fovea of diabetic patients without DR. These results are consistent with previous studies on human central nervous system damage[42] and animal models of glaucoma where retrograde axonal degeneration causes ganglion cell death.[43] In this regard, the ganglion cell death could consequently induce the bipolar cell loss[9] observed in our study. However, it remains unknown whether the degeneration of bipolar cells is a consequence of, or influenced by, the loss of synaptic connectivity in the OPL[39,43] or the death of photoreceptor cells.[44]

Indeed, our findings of ganglion cell degeneration in the DM retinas corroborate the results obtained from OCT measurements of the ganglion cell complex (GCC) and GCL+IPL,[45] as well as the GCL,[46,47] demonstrating the usefulness of OCT in evaluating early changes in these cells. Otherwise, based on the data, ganglion cell degeneration is more pronounced than bipolar cell loss, which may confirm a pattern of degeneration beginning in the inner retina. Moreover, in our study, the density of horizontal cells was preserved in the retinas of the DM group but diminished in the retinas affected by DR, which suggests that the degeneration of horizontal cells follows the loss of bipolar cells.

To our knowledge, this is the first research conducted on neurons of human retinas from diabetic donors, with and without diabetic retinopathy. It highlights the relevance of analyzing synaptic connectivity in diabetic patients without retinopathy and suggests that this neuronal degeneration may contribute to vision impairment in DM. However, most interventional treatments are mainly performed when clinically significant macular edema is present or during the proliferative stages of DR,[5] by which time neuronal degeneration has already significantly progressed according to our results. Indeed, this underscores the need for research into therapies even before structural changes are detected on OCT images or vascular alterations occur. Currently, clinical trials targeting these patients (most with DR) are focused on the use of vitamin supplements, such as vitamin B6/B12, vitamin C, and zinc (www.clinicaltrials.gov; NCT04117022, NCT02062034), as well as antioxidants such as alpha-lipoic acid (NCT01208948) and carotenoids (NCT04117022). The Diabetes Visual Function Supplement Study (DiVFuSS)[48] and the use of carotenoids,[49] alpha-lipoid acid,[50] or vitamin B12[51] have demonstrated improvements in the visual function of diabetic patients. Hence, these results emphasize the importance of implementing early neuroprotective strategies in diabetic patients, even before retinal changes are detected through imaging techniques. This approach may help mitigate the progressive neuronal and glial changes that precede vascular dysfunction.

Acknowledgments

Supported by grants from the Ministerio de Ciencia (FEDER-PID2019-106230RB-I00) and Generalitat Valenciana (IDIFEDER/2017/064, PROMETEO/2021/024) and by the International Center for Aging Research (ICAR).

Disclosure: **H. Albertos-Arranz**, None; **N. Martínez-Gil**, None; **X. Sánchez-Sáez**, None; **J.C. Molina-Martín**, None; **P. Lax**, None; **N. Cuenca**, None

References

1. Schuster DP, Duvuuri V. Diabetes mellitus. *Clin Podiatr Med Surg*. 2002;19(1):79–107.
2. Maraschin JdF. Classification of diabetes. In: Ahmad SI, ed. *Diabetes. Advances in Experimental Medicine and Biology*. New York, NY: Springer; 2012:12–19.
3. Gale MJ, Scruggs BA, Flaxel CJ. Diabetic eye disease: a review of screening and management recommendations. *Clin Exp Ophthalmol*. 2021;49(2):128–145.

4. Guthrie RA, Guthrie DW. Pathophysiology of diabetes mellitus. *Crit Care Nurs Q*. 2004;27(2):113–125.
5. Flaxel CJ, Adelman RA, Bailey ST, et al. Diabetic retinopathy preferred practice pattern. *Ophthalmology*. 2020;127(1):P66–P145.
6. Tang Z, Chan MY, Leung WY, et al. Assessment of retinal neurodegeneration with spectral-domain optical coherence tomography: a systematic review and meta-analysis. *Eye (Lond)*. 2021;35(5):1317–1325.
7. Lecleire-Collet A, Audo I, Aout M, et al. Evaluation of retinal function and flicker light-induced retinal vascular response in normotensive patients with diabetes without retinopathy. *Invest Ophthalmol Vis Sci*. 2011;52(6):2861–2867.
8. Kim M, Kim R, Park W, Park Y, Kim I, Park Y. Electroretinography and retinal microvascular changes in type 2 diabetes. *Acta Ophthalmol*. 2020;98(7):e807–e813.
9. Sohn EH, van Dijk HW, Jiao C, et al. Retinal neurodegeneration may precede microvascular changes characteristic of diabetic retinopathy in diabetes mellitus. *Proc Natl Acad Sci USA*. 2016;113(19):2655.
10. Singh R, Farooq SA, Mannan A, et al. Animal models of diabetic microvascular complications: relevance to clinical features. *Biomed Pharmacother*. 2022;145:112305.
11. Albertos-Arranz H, Martínez-Gil N, Sánchez-Sáez X, et al. Microglia activation and neuronal alterations in retinas from COVID-19 patients: correlation with clinical parameters. *Eye Vis (Lond)*. 2023;10(1):12.
12. Cuenca N, Ortuño-Lizarán I, Sánchez-Sáez X, et al. Interpretation of OCT and OCTA images from a histological approach: clinical and experimental implications. *Prog Retin Eye Res*. 2020;77:100828.
13. Kolb H, Nelson RF, Ahnelt PK, Ortuño-Lizarán I, Cuenca N. The architecture of the human fovea. In: Kolb H, Fernandez E, Nelson R, eds. *Webvision: The Organization of the Retina and Visual System [Internet]*. Salt Lake City, UT: University of Utah Health Sciences Center; 2020. Available at: https://www.ncbi.nlm.nih.gov/books/NBK554706/.
14. Rungger-Brändle E, Dosso AA, Leuenberger PM. Glial reactivity, an early feature of diabetic retinopathy. *Invest Ophthalmol Vis Sci*. 2000;41(7):1971–1980.
15. Nitta A, Murai R, Suzuki N, et al. Diabetic neuropathies in brain are induced by deficiency of BDNF. *Neurotoxicol Teratol*. 2002;24(5):695–701.
16. Furukawa T, Ueno A, Omori Y. Molecular mechanisms underlying selective synapse formation of vertebrate retinal photoreceptor cells. *Cell Mol Life Sci*. 2020;77(7):1251–1266.
17. Dick O, tom Dieck S, Altrock WD, et al. The presynaptic active zone protein bassoon is essential for photoreceptor ribbon synapse formation in the retina. *Neuron*. 2003;37(5):775–786.
18. Bayley PR, Morgans CW. Rod bipolar cells and horizontal cells form displaced synaptic contacts with rods in the outer nuclear layer of the nob2 retina. *J Comp Neurol*. 2007;500(2):286–298.
19. VanGuilder HD, Brucklacher RM, Patel K, Ellis RW, Freeman WM, Barber AJ. Diabetes downregulates presynaptic proteins and reduces basal synapsin I phosphorylation in rat retina. *Eur J Neurosci*. 2008;28(1):1–11.
20. Hombrebueno JR, Chen M, Penalva RG, Xu H. Loss of synaptic connectivity, particularly in second order neurons is a key feature of diabetic retinal neuropathy in the Ins2Akita mouse. *PLoS One*. 2014;9(5):e97970.
21. Stockton RA, Slaughter MM. B-wave of the electroretinogram. A reflection of ON bipolar cell activity. *J Gen Physiol*. 1989;93(1):101–122.
22. Barber AJ, Antonetti DA, Kern TS, et al. The Ins2Akita mouse as a model of early retinal complications in diabetes. *Invest Ophthalmol Vis Sci*. 2005;46(6):2210–2218.
23. Park S-H, Park J-W, Park S-J, et al. Apoptotic death of photoreceptors in the streptozotocin-induced diabetic rat retina. *Diabetologia*. 2003;46(9):1260–1268.
24. Kar D, Kim YJ, Packer O, et al. Volume electron microscopy reveals human retinal mitochondria that align with reflective bands in optical coherence tomography [invited]. *Biomed Opt Express*. 2023;14(10):5512–5527.
25. Silva-Viguera M, García-Romera MC, Bautista-Llamas M. Contrast sensitivity function under three light conditions in patients with type 1 diabetes mellitus without retinopathy: a cross-sectional, case-control study. *Graefes Arch Clin Exp Ophthalmol*. 2023;261(9):2497–2505.
26. Sokol S, Moskowitz A, Skarf B, Evans R, Molitch M, Senior B. Contrast sensitivity in diabetics with and without background retinopathy. *Arch Ophthalmol*. 1985;103(1):51–54.
27. Berkowitz BA. Preventing diabetic retinopathy by mitigating subretinal space oxidative stress in vivo. *Vis Neurosci*. 2020;37:E002.
28. Bearse MA, Ozawa GY. Multifocal electroretinography in diabetic retinopathy and diabetic macular edema. *Curr Diab Rep*. 2014;14(9):526.
29. Kern TS, Berkowitz BA. Photoreceptors in diabetic retinopathy. *J Diabetes Investig*. 2015;6(4):371–380.
30. Ersoz MG, Kırık F, Isik B, Ozdemir H. Henle fiber layer thickness and area measurement in type 2 diabetes mellitus with and without retinopathy using a modified directional optical coherence tomography strategy. *Retina*. 2023;43(7):1097–1106.
31. Martin PM, Roon P, Van Ells TK, Ganapathy V, Smith SB. Death of retinal neurons in streptozotocin-induced diabetic mice. *Invest Ophthalmol Vis Sci*. 2004;45(9):3330–3336.
32. Vujosevic S, Midena E. Retinal layers changes in human preclinical and early clinical diabetic retinopathy support early retinal neuronal and Müller cells alterations. *J Diabetes Res*. 2013;2013:905058.
33. Chen Y, Li J, Yan Y, Shen X. Diabetic macular morphology changes may occur in the early stage of diabetes. *BMC Ophthalmol*. 2016;16:12.
34. van Dijk HW, Kok PHB, Garvin M, et al. Selective loss of inner retinal layer thickness in type 1 diabetic patients with minimal diabetic retinopathy. *Invest Ophthalmol Vis Sci*. 2009;50(7):3404–3409.
35. Orduna-Hospital E, Sanchez-Cano A, Perdices L, Acha J, Lopez-Alaminos EM, Pinilla I. Changes in retinal layers in type 1 diabetes mellitus without retinopathy measured by spectral domain and swept source OCTs. *Sci Rep*. 2021;11(1):10427.
36. Reznicek L, Kernt M, Haritoglou C, Kampik A, Ulbig M, Neubauer AS. In vivo characterization of ischemic retina in diabetic retinopathy. *Clin Ophthalmol*. 2010;5:31–35.
37. Mizutani M, Gerhardinger C, Lorenzi M. Müller cell changes in human diabetic retinopathy. *Diabetes*. 1998;47(3):445–449.
38. Bringmann A, Pannicke T, Grosche J, et al. Müller cells in the healthy and diseased retina. *Prog Retin Eye Res*. 2006;25(4):397–424.
39. Cuenca N, Fernández-Sánchez L, Campello L, et al. Cellular responses following retinal injuries and therapeutic approaches for neurodegenerative diseases. *Prog Retin Eye Res*. 2014;43:17–75.
40. de Hoz R, Rojas B, Ramírez AI, et al. Retinal macroglial responses in health and disease. *Biomed Res Int*. 2016;2016:2954721.
41. Bringmann A, Iandiev I, Pannicke T, et al. Cellular signaling and factors involved in Müller cell gliosis: neuroprotective and detrimental effects. *Prog Retin Eye Res*. 2009;28(6):423–451.

Investigative Ophthalmology & Visual Science

42. de Vries-Knoppert WA, Baaijen JC, Petzold A. Patterns of retrograde axonal degeneration in the visual system. *Brain*. 2019;142(9):2775–2786.
43. Kumar S, Ramakrishnan H, Viswanathan S, Akopian A, Bloomfield SA. Neuroprotection of the inner retina also prevents secondary outer retinal pathology in a mouse model of glaucoma. *Invest Ophthalmol Vis Sci*. 2021;62(9):35.
44. García-Ayuso D, Salinas-Navarro M, Agudo M, et al. Retinal ganglion cell numbers and delayed retinal ganglion cell death in the P23H rat retina. *Exp Eye Res*. 2010;91(6):800–810.
45. Tang Z, Chan MY, Leung WY, et al. Assessment of retinal neurodegeneration with spectral-domain optical coherence tomography: a systematic review and meta-analysis. *Eye (Lond)*. 2021;35(5):1317–1325.
46. van de Kreeke JA, Darma S, Chan Pin Yin JMPL, et al. The spatial relation of diabetic retinal neurodegeneration with diabetic retinopathy. *PLoS One*. 2020;15(4):e0231552.
47. van Dijk HW, Verbraak FD, Kok PHB, et al. Decreased retinal ganglion cell layer thickness in patients with type 1 diabetes. *Invest Ophthalmol Vis Sci*. 2010;51(7):3660–3665.
48. Chous AP, Richer SP, Gerson JD, Kowluru RA. The Diabetes Visual Function Supplement Study (DiVFuSS). *Br J Ophthalmol*. 2016;100(2):227–234.
49. Moschos MM, Dettoraki M, Tsatsos M, Kitsos G, Kalogeropoulos C. Effect of carotenoids dietary supplementation on macular function in diabetic patients. *Eye Vis (Lond)*. 2017;4:23.
50. Gębka A, Serkies-Minuth E, Raczyńska D. Effect of the administration of alpha-lipoic acid on contrast sensitivity in patients with type 1 and type 2 diabetes. *Mediators Inflamm*. 2014;2014:131538.
51. Parisi V, Ziccardi L, Barbano L, Giorno P, Varano M, Parravano M. Citicoline and vitamin B12 eye drops in type 1 diabetes: results of a 36-month pilot study evaluating macular electrophysiological changes. *Adv Ther*. 2021;38(7):3924–3936.